Journal of Hydroscience and Hydraulic Engineering
Vol. 22, No.2 November, 2004, 113-139

Implicit Two-Step Split-Operator Approach for Modelling Two-Dimensional Open Channel Flow

By

T.Y. Hsieh

Research Assistant Professor, Hazard Mitigation Research Center,
National Chiao Tung University, Hsinchu, Taiwan

and

J.C. Yang

Professor, Department of Civil Engineering and Hazard Mitigation Research Center,
National Chiao Tung University, Hsinchu, Taiwan

SYNOPSIS

The objective of this paper is to present a methodology of using an implicit two-step split-operator approach (IM model) for solving the two-dimensional (2D) shallow water flow equations in terms of an orthogonal curvilinear coordinate system. The split-operator procedure involves two steps based on a decomposition of the momentum equations. The first step, dispersion step, is to compute the provisional velocity in the momentum equations without the pressure gradient and bed friction. In the second step, propagation step, the pressure, bed friction and the velocity fields are corrected to satisfy the continuity equation. To demonstrate the need for an implicit scheme for practical use, an explicit type two-step model (EX model) has also been developed herein for comparison. Four cases, including gradually-varied flow, bend flow, shallow recirculating flow and dam-break flow, have been demonstrated to show the accuracy and practical applicability of IM model. A comparison between IM and EX models reveals that the implicit two-step split-operator approach enables the model to be more flexible and efficient for various open-channel problems. The Friedrichs-Courant constraint is relaxed, and hence large time steps can be used to gain computational times with very less numerical instability problems during the simulation.

KEY WORDS: implicit; two-step split-operator approach; shallow water flow equations; depth-averaged model

1. INTRODUCTION

For many hydraulic engineering problems, the analysis of flow in open channels is a fundamental prerequisite. Depth-averaged 2D models are frequently applied to such problems because of their efficiency and considerable accuracy. Typical depth-averaged models have been presented by many researchers such as, McGrirk and Rodi [1], Molls and Chaudhry [2], Ye and McCorquodale [3], and Lien *et al.* [4] etc.

The split-operator (fractional-step or projection) approach is a widely used solution algorithm for solving the incompressible Navier-Stokes equations with primitive variables. The major concept in this approach is that the solution is advanced one time stage in two (or more) steps. Usually, the first step is to compute the provisional velocity in the momentum equations without the pressure gradient. In the second step, i.e., propagation step, the pressure and the velocity fields are corrected to satisfy the continuity equation. Rosenfeld *et al.* [5] used the fractional-step method to solve the unsteady incompressible Navier-Stokes equations in generalized cooridinate systems. Ye and McCorquodale [3] presented a fractional two-step implicit algorithm to the computation of shallow water flows in curvilinear collocated grids.

For order of magnitude analysis, the bed friction is a dominating shear stress in the shallow water flow equations. In order to increase the flexibility of numerical simulation for various hydraulic problems, the propagation step should consider not only the pressure gradient but also the bed friction. Benque *et al.* [6] were the first to use this concept for the computation of 2D tidal current flow in the bay or estuary. Lien *et al.* [4] have showed that when the effect of first step was weak, propagation step model, neglecting the first step, could handle the case well and reduce the CPU time as compared with the complete model.

One of the drawbacks of the split-operator approach for solving the provisional velocity is that it is hard to specify the values of provisional velocity at the boundaries in the incomplete momentum equations [7]. Therefore, reducing the multi- step procedure to the two-step and using an explicit scheme for solving provisional velocity in the first step are the feasible ways to avoid this deficiency [8,4]. However, since the provisional velocity is computed by an explicit scheme, it suffers from the requirement of small computation time steps which depend on the condition of the numerical stability. To relax the time step restriction, one should consider the implicit methods that can allow the use of large time steps.

The purpose of this paper is to present an implicit two-step split-operator approach for solving the shallow water flow equations, in which the provisional velocity is computed implicitly in the first step, then the incomplete momentum equation, which contains the pressure gradient and bed friction, is coupled with the continuity equation in the propagation step to calculate the corrected velocity and the flow depth. Meanwhile, the velocity boundary conditions needed for the dispersion steps adopt the corresponding values from the previous step. In order to examine the stability of the newly-developed implicit two-step split-operator approach model (IM model), an explicit two-step split-operator approach model (EX model) is also developed for comparison, in which the provisional velocity is computed explicitly in the first step. Various hydraulic problems, including gradually-varied flow, bend flow, shallow recirculating flow and dam-break flow have been studied by the proposed IM model. The simulated results are compared with experimental data, analytical solutions and those from EX model to show its practical applicability.

2. GOVERNING EQUATIONS

2.1 Mathematical Formulation

The following assumptions are made: (1) incompressible Newtonian fluid; (2) hydrostatic pressure distribution; (3) negligible wind shear at the water surface; (4) negligible Coriolis acceleration. The governing equations in 3D form are integrated over the depth to obtain the 2D conservative depth-averaged equations in orthogonal curvilinear coordinates as follows:

Continuity equation

$$h_1 h_2 \frac{\partial d}{\partial t} + \frac{\partial}{\partial \xi}(h_2 \bar{\bar{u}} d) + \frac{\partial}{\partial \eta}(h_1 \bar{\bar{v}} d) = 0 \tag{1}$$

Momentum equations

$$\begin{aligned}
&\frac{\partial \bar{\bar{u}}}{\partial t} + \frac{\bar{\bar{u}}}{h_1}\frac{\partial \bar{\bar{u}}}{\partial \xi} + \frac{\bar{\bar{v}}}{h_2}\frac{\partial \bar{\bar{u}}}{\partial \eta} + \frac{1}{h_1 h_2}\frac{\partial h_1}{\partial \eta}\overline{\overline{uv}} - \frac{1}{h_1 h_2}\frac{\partial h_2}{\partial \xi}\bar{\bar{v}}^2 \\
&= -\frac{g}{h_1}\frac{\partial}{\partial \xi}(z_b + d) + \frac{1}{\rho h_1 h_2 d}\frac{\partial}{\partial \xi}(h_2 T_{11}) + \frac{1}{\rho h_1 h_2 d}\frac{\partial}{\partial \eta}(h_1 T_{12}) \\
&+ \frac{1}{\rho h_1 h_2 d}\frac{\partial h_1}{\partial \eta}T_{12} - \frac{1}{\rho h_1 h_2 d}\frac{\partial h_2}{\partial \xi}T_{22} - \frac{\tau_{b_1}}{\rho d} + \frac{1}{\rho h_1 h_2 d}\left[-(h_2\tau_{11})_s\frac{\partial z_s}{\partial \xi}\right. \\
&\left. + (h_2\tau_{11})_b\frac{\partial z_b}{\partial \xi} - (h_1\tau_{12})_s\frac{\partial z_s}{\partial \eta} + (h_1\tau_{12})_b\frac{\partial z_b}{\partial \eta}\right]
\end{aligned} \tag{2}$$

$$\begin{aligned}
&\frac{\partial \bar{\bar{v}}}{\partial t} + \frac{\bar{\bar{u}}}{h_1}\frac{\partial \bar{\bar{v}}}{\partial \xi} + \frac{\bar{\bar{v}}}{h_2}\frac{\partial \bar{\bar{v}}}{\partial \eta} + \frac{1}{h_1 h_2}\frac{\partial h_2}{\partial \xi}\overline{\overline{uv}} - \frac{1}{h_1 h_2}\frac{\partial h_1}{\partial \eta}\bar{\bar{u}}^2 \\
&= -\frac{g}{h_2}\frac{\partial}{\partial \eta}(z_b + d) + \frac{1}{\rho h_1 h_2 d}\frac{\partial}{\partial \xi}(h_2 T_{12}) + \frac{1}{\rho h_1 h_2 d}\frac{\partial}{\partial \eta}(h_1 T_{22}) \\
&- \frac{1}{\rho h_1 h_2 d}\frac{\partial h_1}{\partial \eta}T_{11} + \frac{1}{\rho h_1 h_2 d}\frac{\partial h_2}{\partial \xi}T_{12} - \frac{\tau_{b_2}}{\rho d} + \frac{1}{\rho h_1 h_2 d}\left[-(h_2\tau_{12})_s\frac{\partial z_s}{\partial \xi}\right. \\
&\left. + (h_2\tau_{12})_b\frac{\partial z_b}{\partial \xi} - (h_1\tau_{22})_s\frac{\partial z_s}{\partial \eta} + (h_1\tau_{22})_b\frac{\partial z_b}{\partial \eta}\right]
\end{aligned} \tag{3}$$

in which

$$T_{11} = \int_{z_b}^{z_s} [\tau_{11} - \rho\overline{u'^2} - \rho(\bar{u} - \bar{\bar{u}})^2]dz \tag{4}$$

$$T_{22} = \int_{z_b}^{z_s} [\tau_{22} - \rho\overline{v'^2} - \rho(\bar{v} - \bar{\bar{v}})^2]dz \tag{5}$$

$$T_{12} = T_{21} = \int_{z_b}^{z_s} [\tau_{12} - \rho\overline{u'v'} - \rho(\bar{u} - \bar{\bar{u}})(\bar{v} - \bar{\bar{v}})]dz \tag{6}$$

where ξ and η = orthogonal curvilinear coordinates in the streamwise axis and transverse axis, respectively; h_1 and h_2 =metric coefficients in ξ- and η- directions, respectively; u and v = velocity components in ξ- and η- direction, respectively; ρ = fluid density; g = gravitational acceleration; t = the time; d = depth; z_b = bed elevation; z_s = water surface elevation; overbar ($\bar{}$) = time average; double overbar ($\bar{\bar{}}$) = depth average; prime (') = fluctuating component; and subscripts s and b indicate the dependent variables at the water surface and channel bed, respectively. The effective stresses (T_{11}, T_{12}, T_{22}) act tangentially to the vertical sides of a fluid element and consist of laminar viscous stresses, turbulent stresses, and dispersion stresses due to depth-averaged operations.

2.2 Closure Model —Quantifying Stress Terms

To solve (1)-(3) as a closed system, the stress terms on the right-hand side of (2) and (3) have to be expressed as explicit functions of the depth-averaged velocities and the depth.

The bottom shear stresses τ_{b1}, τ_{b2} are modeled according to the following formulas [9]

$$\tau_{b_1} = C_f \rho \bar{\bar{u}} (\bar{\bar{u}}^2 + \bar{\bar{v}}^2)^{1/2} \tag{7}$$

$$\tau_{b_2} = C_f \rho \bar{\bar{v}} (\bar{\bar{u}}^2 + \bar{\bar{v}}^2)^{1/2} \tag{8}$$

where $C_f = g/c^2$ = friction factor; and c = Chezy factor.

The laminar viscous stresses and turbulent stresses will be quantified in accordance with the Boussinesq eddy-viscosity concept, which can be expressed as

$$\frac{\tau_{11}}{\rho} - \overline{u'^2} = 2\upsilon\left[\frac{1}{h_1}\frac{\partial \bar{u}}{\partial \xi} + \frac{\bar{v}}{h_1 h_2}\frac{\partial h_1}{\partial \eta}\right] \tag{9}$$

$$\frac{\tau_{22}}{\rho} - \overline{v'^2} = 2\upsilon\left[\frac{1}{h_2}\frac{\partial \bar{v}}{\partial \eta} + \frac{\bar{u}}{h_1 h_2}\frac{\partial h_2}{\partial \xi}\right] \tag{10}$$

$$\frac{\tau_{12}}{\rho} - \overline{u'v'} = 2\upsilon\left[\frac{h_2}{h_1}\frac{\partial}{\partial \xi}\left(\frac{\bar{v}}{h_2}\right) + \frac{h_1}{h_2}\frac{\partial}{\partial \eta}\left(\frac{\bar{u}}{h_1}\right)\right] \tag{11}$$

where $\upsilon = \upsilon_l + \upsilon_t$; υ_l = laminar kinematic viscosity; υ_t = turbulent kinematic viscosity $= kU_* d/6$ [10]; $U_* = (\tau_b/\rho)^{1/2}$ = shear velocity; k = von Karman's constant (about 0.4).

Integrals along the vertical direction of velocity deviations from depth-averaged values represent the dispersion stress terms. In the present study, only the secondary current effect is considered in the dispersion stress terms. The velocity profiles in the streamwise and transverse directions proposed by de Vriend [11] are adopted in the present study

$$\bar{u} = \bar{\bar{u}}\left[1 + \frac{\sqrt{g}}{kc} + \frac{\sqrt{g}}{kc}\ln\zeta\right] = \bar{\bar{u}} f_m(\zeta) \tag{12}$$

$$\bar{v} = \bar{\bar{v}} f_m(\zeta) + \frac{\bar{\bar{u}} d}{k^2 r}\left[2F_1(\zeta) + \frac{\sqrt{g}}{kc}F_2(\zeta) - 2(1 - \frac{\sqrt{g}}{kc}) f_m(\zeta)\right] \tag{13}$$

in which

$$F_1(\zeta) = \int_0^1 \frac{\ln\zeta}{\zeta - 1} d\zeta \tag{14}$$

$$F_2(\zeta) = \int_0^1 \frac{(\ln\zeta)^2}{\zeta - 1} d\zeta \tag{15}$$

where $\varsigma = (z - z_b)/d$ = dimensionless distance from the bed; and r = radius of curvature.

3. NUMERICAL ALGORITHM

The two-step split-operator approach involves two steps based on a decomposition of the momentum equations. The first step (called the dispersion step) is to compute the provisional velocity in the momentum equation without the pressure gradient and bed friction. In the second step-the propagation step-the pressure, bed friction and the velocity fields are corrected to satisfy the continuity equation. The only difference between the IM and the EX models is the treatment of numerical scheme in the dispersion step. IM model uses the implicit scheme and EX model uses the explicit scheme. They can be expressed sequentially in the vector form as follows:

Dispersion step

For IM model

$$\left(\frac{\partial V}{\partial t}\right)^{n+\frac{1}{2}} = -(V^{n+\frac{1}{2}} \cdot \nabla)V^{n+\frac{1}{2}} + \frac{1}{\rho}\nabla \cdot T^{n+\frac{1}{2}} \tag{16}$$

For EX model

$$\left(\frac{\partial V}{\partial t}\right)^{n+\frac{1}{2}} = -(V^{n} \cdot \nabla)V^{n} + \frac{1}{\rho}\nabla \cdot T^{n} \tag{17}$$

Propagation step

$$\left(\frac{\partial V}{\partial t}\right)^{n+1} - \left(\frac{\partial V}{\partial t}\right)^{n+\frac{1}{2}} = -g\nabla(z_b + d)^{n+1} - \frac{\tau_b}{\rho d} \tag{18}$$

$$\nabla \cdot V^{n+1} = 0 \tag{19}$$

where the superscript $n+1$ denotes the unknown variables at time level $(n+1)\Delta t$; the superscript n denotes the known variables at time level n; the superscript $n+\frac{1}{2}$ denotes the unknown variables at intermediate time level between steps.

One can express the above equations again in the following forms and drop the double overbar to simplify the notation of depth-averaging for velocity variables.

Dispersion step

$$\frac{\partial u}{\partial t} = -\frac{u}{h_1}\frac{\partial u}{\partial \xi} - \frac{v}{h_2}\frac{\partial u}{\partial \eta} - \frac{1}{h_1 h_2}\left[\frac{\partial h_1}{\partial \eta}uv - \frac{\partial h_2}{\partial \xi}v^2\right] + \frac{1}{\rho h_1 h_2 d}\frac{\partial (h_2 T_{11})}{\partial \xi}$$

$$+\frac{1}{\rho h_1 h_2 d}\frac{\partial(h_1 T_{12})}{\partial \eta}+\frac{1}{\rho h_1 h_2 d}\frac{\partial h_1}{\partial \eta}T_{12}-\frac{1}{\rho h_1 h_2 d}\frac{\partial h_2}{\partial \xi}T_{22}+\frac{1}{\rho h_1 h_2 d}\left[-(h_2\tau_{11})_s\frac{\partial z_s}{\partial \xi}\right.$$

$$\left.+(h_2\tau_{11})_b\frac{\partial z_b}{\partial \xi}-(h_1\tau_{12})_s\frac{\partial z_s}{\partial \eta}+(h_1\tau_{12})_b\frac{\partial z_b}{\partial \eta}\right] \tag{20}$$

$$\frac{\partial v}{\partial t}=-\frac{u}{h_1}\frac{\partial v}{\partial \xi}-\frac{v}{h_2}\frac{\partial v}{\partial \eta}-\frac{1}{h_1 h_2}\left[\frac{\partial h_2}{\partial \xi}uv+\frac{\partial h_1}{\partial \eta}u^2\right]+\frac{1}{\rho h_1 h_2 d}\frac{\partial(h_2 T_{12})}{\partial \xi}$$

$$+\frac{1}{\rho h_1 h_2 d}\frac{\partial(h_1 T_{22})}{\partial \eta}-\frac{1}{\rho h_1 h_2 d}\frac{\partial h_1}{\partial \eta}T_{11}+\frac{1}{\rho h_1 h_2 d}\frac{\partial h_2}{\partial \xi}T_{12}+\frac{1}{\rho h_1 h_2 d}\left[-(h_2\tau_{12})_s\frac{\partial z_s}{\partial \xi}\right.$$

$$\left.+(h_2\tau_{12})_b\frac{\partial z_b}{\partial \xi}-(h_1\tau_{22})_s\frac{\partial z_s}{\partial \eta}+(h_1\tau_{22})_b\frac{\partial z_b}{\partial \eta}\right] \tag{21}$$

Propagation step

$$\frac{\partial u}{\partial t}=-\frac{g}{h_1}\left(\frac{\partial(z_b+d)}{\partial \xi}\right)-\frac{C_f u\sqrt{u^2+v^2}}{d} \tag{22}$$

$$\frac{\partial v}{\partial t}=-\frac{g}{h_2}\left(\frac{\partial(z_b+d)}{\partial \eta}\right)-\frac{C_f v\sqrt{u^2+v^2}}{d} \tag{23}$$

and

$$h_1 h_2\frac{\partial d}{\partial t}+\frac{\partial(h_2 u d)}{\partial \xi}+\frac{\partial(h_1 v d)}{\partial \eta}=0 \tag{24}$$

Using a Taylor series expansion for water depth, d^{n+1}, and retaining the first-order terms only, one can easily obtain the linearized expressions of (24) as follows:

$$h_1 h_2\frac{\partial d}{\partial t}+\frac{\partial}{\partial \xi}\left(\alpha_1\frac{\partial(\Delta d)}{\partial \xi}+\beta_1\Delta d+\gamma_1\right)+\frac{\partial}{\partial \eta}\left(\alpha_2\frac{\partial(\Delta d)}{\partial \eta}+\beta_2\Delta d+\gamma_2\right)=0 \tag{25}$$

where

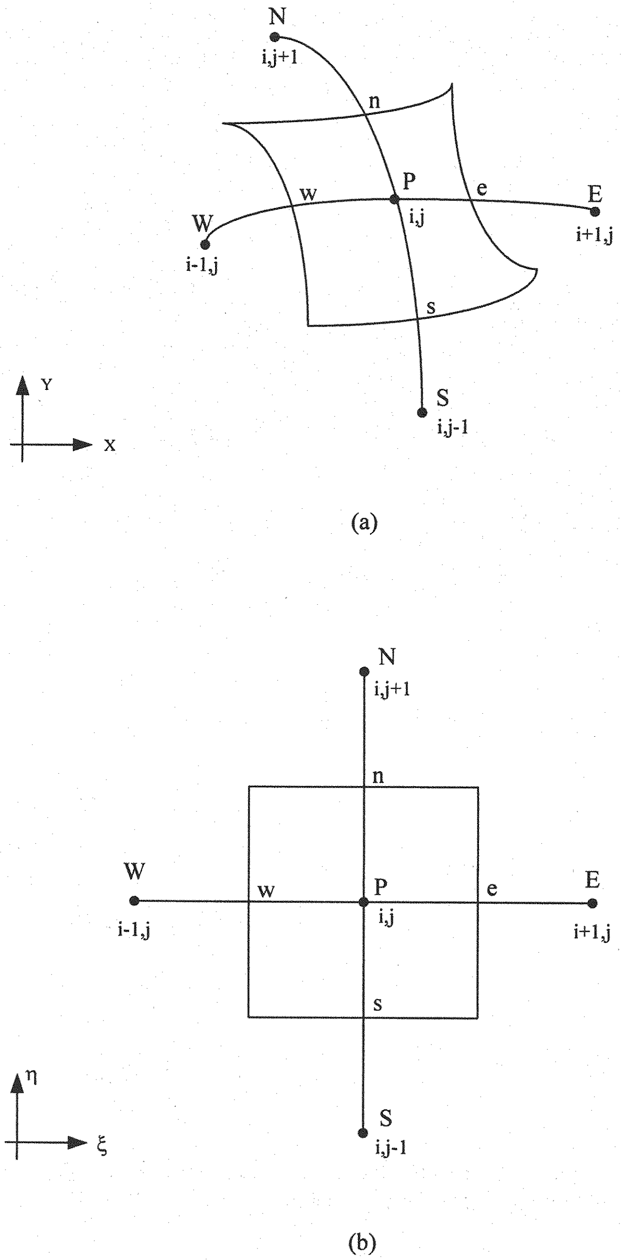

Fig. 1 Control volume in: (a) physical plane; (b) computational plane

$$\alpha_1 = -\frac{h_2 g \Delta t}{C_\tau h_1} d^n ; \qquad \beta_1 = \frac{h_2}{C_\tau} u^{n+\frac{1}{2}} - \frac{h_2 g \Delta t}{C_\tau h_1} [\frac{\partial z_b^{n+1}}{\partial \xi} + \frac{\partial d^n}{\partial \xi}] ; \quad \gamma_1 = \beta_1 d^n \tag{26}$$

$$\alpha_2 = -\frac{h_1 g \Delta t}{C_\tau h_2} d^n ; \qquad \beta_2 = \frac{h_1}{C_\tau} v^{n+\frac{1}{2}} - \frac{h_1 g \Delta t}{C_\tau h_2} [\frac{\partial z_b^{n+1}}{\partial \eta} + \frac{\partial d^n}{\partial \eta}] ; \quad \gamma_2 = \beta_2 d^n \tag{27}$$

$$C_\tau = 1 + \Delta t \frac{C_f \sqrt{(u^{n+\frac{1}{2}})^2 + (v^{n+\frac{1}{2}})^2}}{d^n} \tag{28}$$

where $\Delta d = d^{n+1} - d^n$; $\Delta t = t^{n+1} - t^n$.

3.1 Discretized Equations

The working equations of each step are discretized by using the finite-volume method. A typical control volume for node P for both physical and computational plane is shown in Fig. 1, where the capital letters E, W, N and S denote the neighboring nodes; and the lowercase letters e, w, n and s denote the control volume faces. The discretized forms of the governing equations are given in the following paragraphs.

The general form of the governing equations is integrated over the control volume $\Delta\xi\Delta\eta$ of node P. The present study uses the forward difference scheme to discretize the time derivatives. All of the spatial derivatives are estimated with central difference of second-order accuracy, except the advection terms whose face values represented in terms of nodal values can be obtained by the Hybrid scheme [12] which combines the central difference and the upwind scheme to catch the direction of fluid flow.

The central difference scheme used here can be written as follows:

$$\left(\frac{\partial \Psi}{\partial \xi}\right)_P^m = \frac{\Psi_e^m - \Psi_w^m}{\Delta \xi} \tag{29}$$

$$\left(\frac{\partial \Psi}{\partial \eta}\right)_P^m = \frac{\Psi_n^m - \Psi_s^m}{\Delta \eta} \tag{30}$$

where

$$\Psi_e^m = 0.5 \cdot (\Psi_E^m + \Psi_P^m) = 0.5 \cdot (\Psi_{i+1,j}^m + \Psi_{i,j}^m) \tag{31}$$

$$\Psi_w^m = 0.5 \cdot (\Psi_P^m + \Psi_W^m) = 0.5 \cdot (\Psi_{i,j}^m + \Psi_{i-1,j}^m) \tag{32}$$

$$\Psi_n^m = 0.5 \cdot (\Psi_N^m + \Psi_P^m) = 0.5 \cdot (\Psi_{i,j+1}^m + \Psi_{i,j}^m) \qquad (33)$$

$$\Psi_s^m = 0.5 \cdot (\Psi_P^m + \Psi_S^m) = 0.5 \cdot (\Psi_{i,j}^m + \Psi_{i,j-1}^m) \qquad (34)$$

where Ψ could stand for u, v, h_1, h_2, d, z_s and z_b; in the dispersion step, superscript m represents n for EX model and $n+\frac{1}{2}$ for IM model; in the propagation step, superscript m represents $n+1$.

The Hybrid scheme is used herein for calculating the advection terms which can be written as follows:

$$\frac{u^d}{h_1}\left(\frac{\partial \Phi^m}{\partial \xi}\right) = 0.5\frac{u_{i,j}^d}{h_{1i,j}}\left[(1-\alpha_x)\left(\frac{\Phi_{i+1,j}^m - \Phi_{i,j}^m}{\Delta\xi}\right) + (1+\alpha_x)\left(\frac{\Phi_{i,j}^m - \Phi_{i-1,j}^m}{\Delta\xi}\right)\right] \qquad (35)$$

$$\frac{v^d}{h_2}\left(\frac{\partial \Phi^m}{\partial \eta}\right) = 0.5\frac{v_{i,j}^d}{h_{2i,j}}\left[(1-\alpha_y)\left(\frac{\Phi_{i,j+1}^m - \Phi_{i,j}^m}{\Delta\eta}\right) + (1+\alpha_y)\left(\frac{\Phi_{i,j}^m - \Phi_{i,j-1}^m}{\Delta\eta}\right)\right] \qquad (36)$$

where

$$\alpha_x = \begin{cases} 0 & |R_x| \le 2 \\ 1 & R_x > 2 \\ -1 & R_x < -2 \end{cases} \quad ; \quad \alpha_y = \begin{cases} 0 & |R_y| \le 2 \\ 1 & R_y > 2 \\ -1 & R_y < -2 \end{cases} \qquad (37)$$

$$R_x = \frac{u_{i,j}^n h_{1i,j} \Delta\xi}{\mu/\rho} \quad ; \quad R_y = \frac{v_{i,j}^n h_{2i,j} \Delta\eta}{\mu/\rho} \qquad (38)$$

where Φ could stand for u or v; μ is the fluid dynamic viscosity; superscript d represents n for EX model and the velocity values from the previous iteration are adopted to correct the nonlinear terms in IM model .

The mesh Reynolds number (R_x or R_y) is introduced in the algorithm to help select the proper finite difference mode for computing the advection terms. The central difference is used in the low mesh Reynolds number and the upwind scheme is used in the high mesh Reynolds number. The upwind scheme uses backward difference when the velocity is positive and uses forward difference when the velocity is negative. The hybrid scheme provides the first order accuracy against upwind scheme and second order accuracy against the central difference in the space.

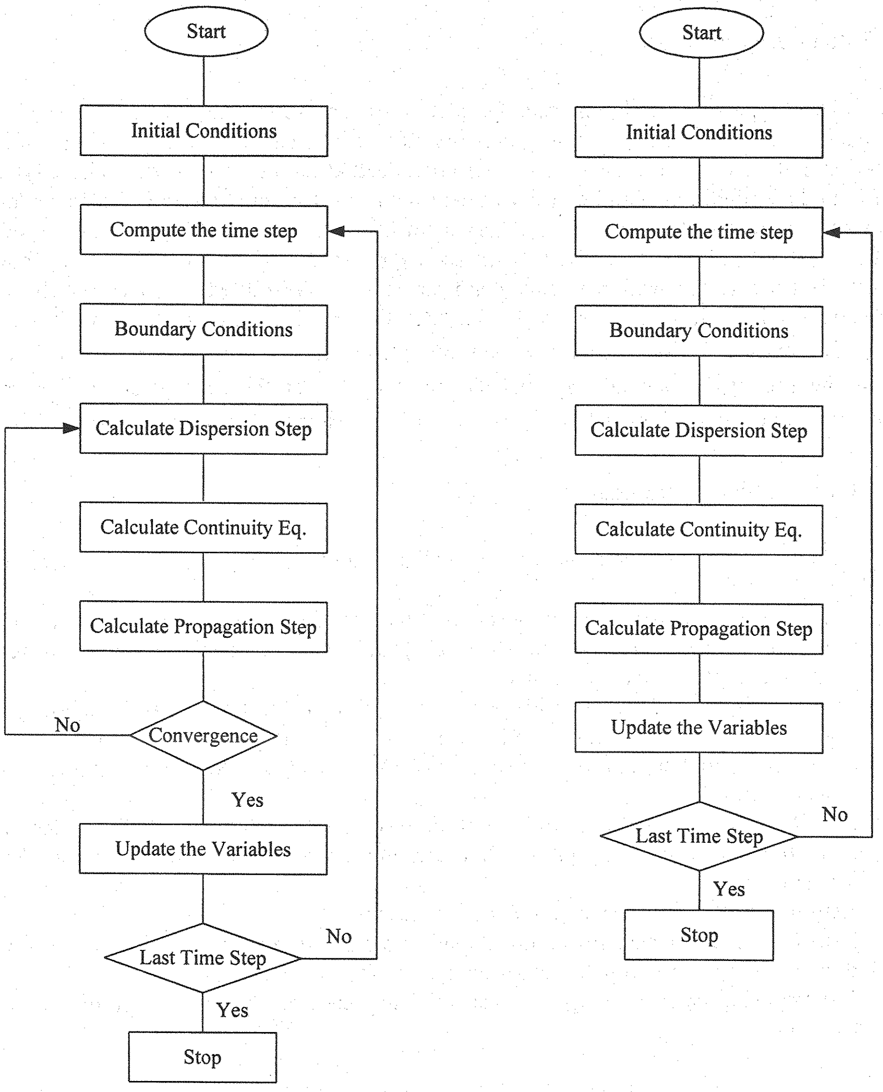

(a) IM model

(b) EX model

Fig. 2 Flow chart for IM and EX models

3.2 Boundary Conditions

Three types of boundaries, namely, inlet, outlet and solid walls are considered. In general, the unit discharge hydrograph per unit width can be specified at the inlet section and water-surface elevation can be specified at the outlet section. These types of boundary conditions can be easily transformed into the function with the dependent variables in terms of the depth-increment as in (25). At the solid boundaries, the law of the wall is applied outside the viscous sublayer and transition layer. The wall shear stress is used as the wall boundary condition and is substituted into the momentum equation in the wall region to solve for the velocity component parallel to the wall.

The extra velocity boundary conditions needed for dispersion step, u_Γ^d and v_Γ^d must be specified when an implicit scheme is used. For the sake of simplicity, the previous time- step values $u_\Gamma^d = u_\Gamma^n$ and $v_\Gamma^d = v_\Gamma^n$ are adopted as the boundary.

3.3 Overall Solution Procedure

The solution procedures for solving shallow water flow equations can be listed as follows:

1. Calculate the provisional velocities explicitly (for EX model) or implicitly (for IM model) from the momentum equations (20) and (21) without the pressure gradient terms to complete the dispersion step.
2. Compute Equation (25) implicitly to obtain depth increment by the ADI method.
3. The unknown velocities are calculated by correcting the provisional velocities with the pressure gradient and bed friction from Equations (22) and (23) to complete the propagation step.
4. For IM model, 1-3 steps are required to compute repeatedly until successive predictions of velocities and depth increment no longer change along the flow domain.
5. Return to step 1 and proceed to the next time step.
6. Repeat the above procedures until a steady state solution is reached (for steady state flows) or the specific time period is completed (for unsteady flows).
7. The flow chart shown in Fig. 2 explains the sequence of tasks performed by EX and IM models.

4. APPLICATIONS

In order to verify the capability of the IM model, four cases, including gradually-varied flow, bend flow, shallow recirculating flow and dam-break flow, are studied herein. The simulated results are compared with experimental data or analytical solution to show the accuracy of the model. Moreover, the numerical stability for both IM and EX models are examined to show the practical applicability of IM model. In all cases, the grid systems are designed to be fine enough to meet the requirement of sufficient accuracy. With regard to the model's convergence, the following criteria should be satisfied:

$$\max\left[\left(\Omega_{i,j}^{n+1} - \Omega_{i,j}^{n}\right)\right] \le 1.0\times10^{-3} \tag{39}$$

where Ω could stand for u, or v, or d at each grid point.

4.1 Gradually-Varied Flow Case

The computation of gradually-varied flow (GVF) is one of the standard tests to examine the proposed model for the shallow water flow. The present study considers a hypothetical GVF case for a 8000-m-long straight, rectangular channel with the following parameters: a width of 100 m, a slope of 0.0005, and Manning's roughness of 0.035. The steady unit discharge 3.987 m^2/s was specified at the channel inlet. The water depth was raised to 4.5 m by means of a low weir at the channel outlet. The normal depth and critical depth of this flow is 3.0 m and 1.175 m, respectively. The uniform mesh of 81×11 are used in the present simulation.

The simulated variations of flow depth and longitudinal velocity obtained from IM model (Δt = 100 s) show that the flow depth gradually varies from 4.5 m at the weir site to 3.05 m at the upstream end, which is close to the normal depth, and this water-surface profile can be described as an M_1 curve. Consequently, the velocity varies from 0.886 m/s to 1.307 m/s corresponding to the variation of flow depth from downstream to upstream.

Table 1 CPU time needed by IM and EX models for GVF case with various Δt

Δt(sec)	5		10		50		100		112		$1\text{x}10^3$	$1\text{x}10^4$
Model Type	EX	IM	EX	IM	EX	IM	EX	IM	EX	IM	IM	IM
CPU Time (sec)	4787	5319	2397	2666	482	533	237	267	214	238	27.1	2.7
Max CFL	0.07		0.13		0.65		1.31		1.46		13.00	128.8
$\overline{CFL}$	0.05		0.09		0.47		0.94		1.06		9.36	458.1

Various time steps were selected to examine the stability of IM and EX models. The CPU time for 10 days' simulation, *Max CFL*, and $\overline{CFL}$ for each case are shown in Table1, in which *CFL* (Courant-Friedichs-Lewy number) at a grid point can be defined as $CFL_{i,j}$ = $\left(\left|u_{i,j}\right|/\Delta x_{i,j} + \left|v_{i,j}\right|/\Delta y_{i,j}\right)\cdot \Delta t$; $Max\ CFL$ = $Max\left(CFL_{i,j}\right)$, where Max represent the maximum value for all the grid points; and $\overline{CFL}$ = $\sum_{1}^{N} CFL_{i,j} / N$, where N represents the total grid numbers. The computations presented in the present paper were all executed on an IBM SP2 SMP machine. In order to examine the accuracy of the simulated results, three reliability parameters, including root mean square error, E_{rms}; geometric reliability index, k_g; and statistical reliability index, k_s, are defined below:

$$E_{rms} = \left(\frac{\sum_{N_{total}} \left(X_{i,j} - Y_{i,j} \right)^2}{N_{total}} \right)^{1/2} \tag{40}$$

$$k_g = \frac{1 + \sqrt{\frac{1}{N_{total}} \sum_{i=1}^{N_{total}} \left[\frac{1-(Y_{i,j}/X_{i,j})}{1+(Y_{i,j}/X_{i,j})} \right]^2}}{1 - \sqrt{\frac{1}{N_{total}} \sum_{i=1}^{N_{total}} \left[\frac{1-(Y_{i,j}/X_{i,j})}{1+(Y_{i,j}/X_{i,j})} \right]^2}} \tag{41}$$

$$k_s = \exp\left\{ \sqrt{\frac{1}{N_{total}} \sum_{i=1}^{N_{total}} \left[\log\left(\frac{Y_{i,j}}{X_{i,j}} \right) \right]^2} \right\} \tag{42}$$

where $X_{i,j}$ denotes the simulated result at comparative point; $Y_{i,j}$ denotes the observed result at comparative point; N_{total} denotes the total numbers of point compared.

E_{rms} represents the averaged error between the simulated results and the observed results. k_g and k_s were proposed by Leggett and Williams [13] as a criteria to determine the reliability of a model or to select the appropriate model. As pointed out by Leggett and Williams [13], the model predicts the observed results reasonably well when the value of the ratio k_g / k_s lies between 0.989 and 1.027. In the present study, the influence on the flow field by the transverse velocity is not significant since the orthogonal curvilinear coordinates system is used. Therefore, the use of these indexes will only focus on the depth and the longitudinal velocity.

For this simple backwater computation case, it is possible to arbitrarily pick up any results from model as the observed results. Here, the results from IM model with Δt = 100 s are taken as the observed results for the calculation of reliability parameters. From the results, it has been found that the values of E_{rms} almost approach to zero (say less than 1.5×10^{-4}) and the ratio k_g / k_s all lie between the reliable range as indicated by Leggett and Williams [13] for each case studied here. From Table 1, one can observe that the maximum time step allowed for EX model is 112 s; for this case the *Max CFL* is 1.46 and $\overline{CFL}$ is 1.06. Meanwhile, the use of IM model allows very large *Max CFL* and $\overline{CFL}$ values and almost achieves unconditionally stable. Though the dispersion step plays almost no role in the GVF case, as pointed out by Lien *et al.* [4], the main disadvantage of EX model that lies in the restriction on the time step is still obvious. Furthermore, if the maximum allowable Δt = 112 s is used for EX model and Δt = 1×10^4 s is used for IM model, the CPU time needed for IM model is almost 80 times less than that for EX model.

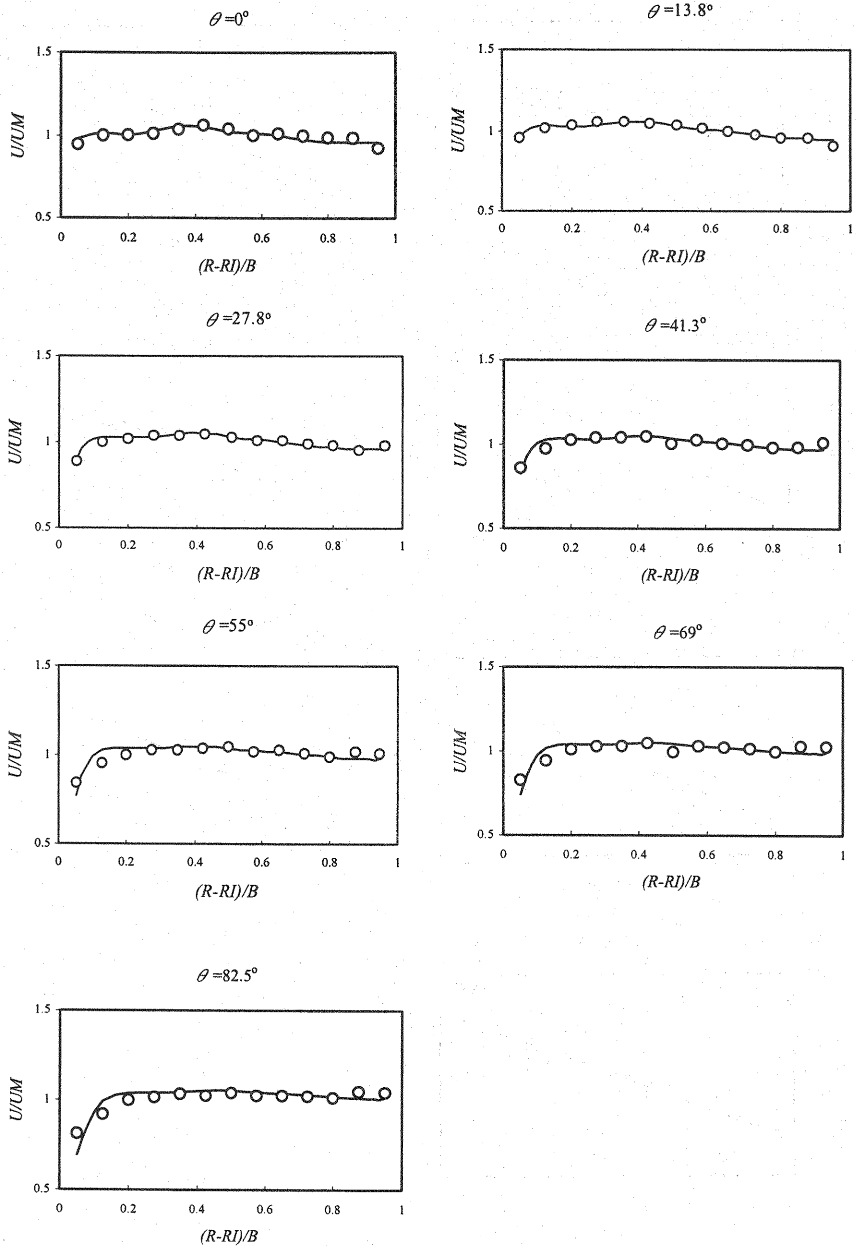

Fig. 3 Velocity ratio U/UM across dimensionless channel width for de Vriend and Koch's simulation. Measured (○); IM model (—).

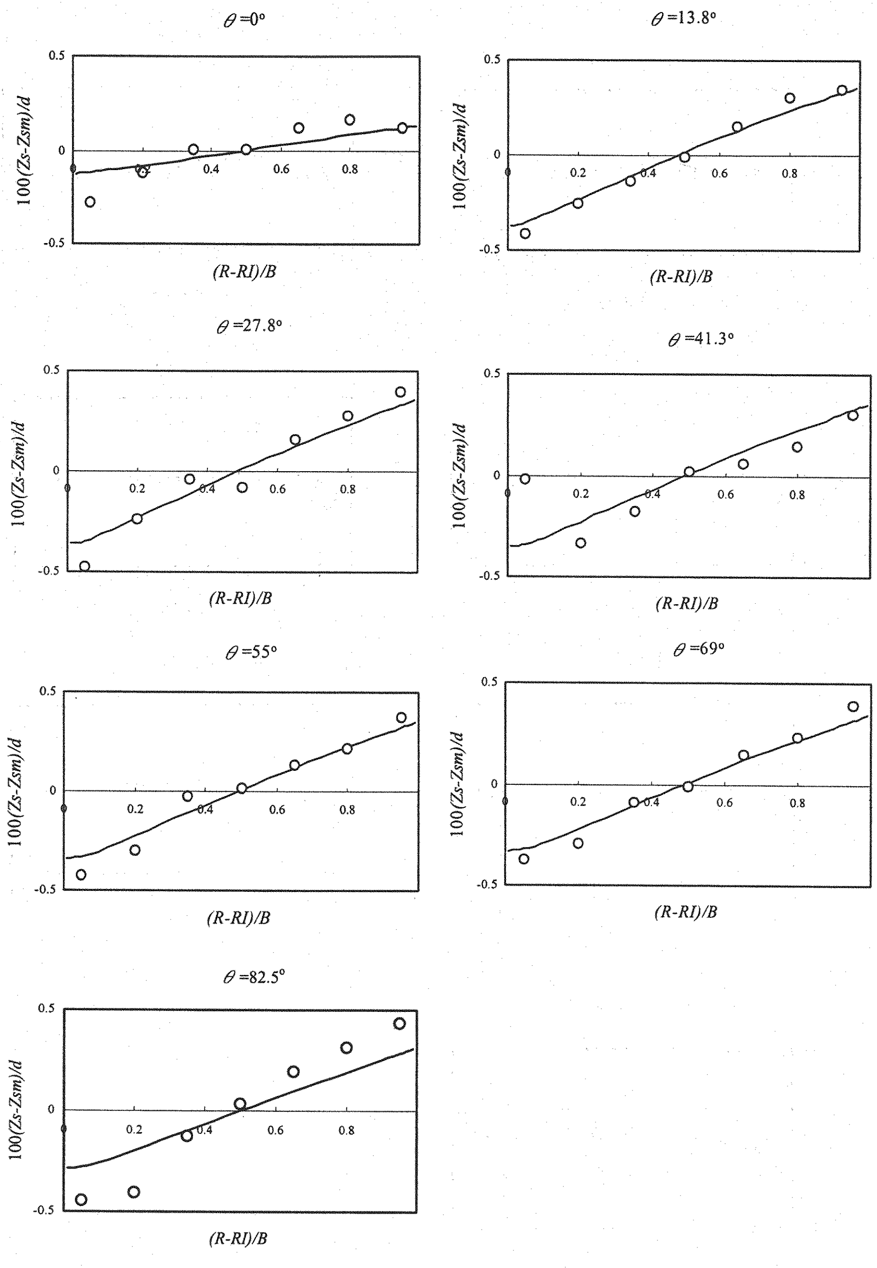

Fig. 4 Depth Ratio $100\cdot(Z_s - Z_{sm})/d$ across dimensionless channel width for de Vriend and Koch's simulation. Measured (○); IM model (—).

4.2 Bend Flow Case

One of the riddles of nature is the meandering of rivers. Predicting the hydrodynamic processes in bends is of vital importance, since such knowledge is helpful in making use of rivers, such as navigation, water supply, waste discharge, flood control and so on.

IM model is validated by comparing the simulated results with experimental data obtained by de Vriend and Koch [14]. In de Vriend and Koch's experiment, the channel consisted of a 39-m long straight section followed by a 90° bend with a radius of curvature of 50 m. The channel cross section was rectangular, and the width was 6 m. The channel bed was horizontal in the straight portion and had a slope of 3×10^{-4} in the curved portion. The Chezy factor was 70 $m^{1/2}/s$. The discharge given from the upstream end of the channel was 0.61 m^3/s; yielding the average velocity was about 0.4 m/s, and the average flow depth was 0.25 m.

The mesh of 103×39 was used in the simulation. The simulation reach covered a 23-m-long straight channel before the entrance of the bend and a 90° bend with a radius of curvature of 50 m. The upstream boundary condition was the inflow discharge per unit width, and the downstream boundary condition was the measured water-surface elevation and no-slip boundary was used at the banks.

Fig. 3 shows the variation of velocity ratios U/UM across the dimensionless channel width $[(r-r_i)/B]$ obtained from IM model (Δt = 2.59 s) and the measured data, where U is the depth-averaged longitudinal velocity, UM is cross-section averaged longitudinal velocity, r_i is the radius of curvature of the inner bank and B is the channel width. Fig. 4 shows the corresponding dimensionless depth ratio $100\cdot(z_s-z_{sm})/d$ against the dimensionless channel width, where z_{sm} is the mean water-surface elevation across the channel width. One can observe from Figs. 3 and 4 that the simulated results agree fairly well with measured data. In Fig. 3, the longitudinal velocity near the outer bank increases along the bend and becomes greater than that near the inner bank due to the transverse convection of streamwise momentum along the bend caused by the secondary current. The velocity becomes lower near the inner bank and higher near the outer bank starting from the $\theta = 27.8^{\circ}$ section. This phenomenon becomes more evident as the flow moves further downstream. In Fig. 4, the superelevation water surface in the bend can be observed even at the entrance to the bend, which is $\theta = 0^{\circ}$. As expected, the water surface is higher at the outer bank than at the inner bank in the channel bend. The stable transverse slope of the water surface is established soon after the beginning of the bend ($\theta = 13.8^{\circ}$).

Table 2 CPU time needed by IM and EX models for bend flow case with various Δt

Δt(sec)	0.5		1		2.59		4	6	8	9.45
Model Type	EX	IM	EX	IM	EX	IM	IM	IM	IM	IM
CPU Time (sec)	2112	2412	1066	1250	446	519	357	277	234	154
Max CFL	0.33		0.61		1.49		2.88	4.63	6.56	8.07
$\overline{CFL}$	0.18		0.35		0.91		1.41	2.12	2.83	3.35

Table 2 shows the results of stability status for simulating the bend flow case with IM and EX models. From the previous validation analysis, the results obtained from IM model with Δt = 2.59 s, which agree very well with measured data, are thought to be reasonably considered as observed results. Consequently, it was found that E_{rms} almost approaches zero (say less than 2.5×10^{-3}) and the values of the ratio k_g/k_s all lie between 0.989 and 1.027 for each case studied here. From Table 2, one can observe that the use of the EX model cause a restriction on the allowing maximum time step that is 2.59 s and correspondingly yields *Max CFL* of 1.49 and $\overline{CFL}$ of 0.91. Not like the GVF case, here IM model is no longer unconditionally stable, in which the maximum time step allowed is 9.45 s and the *Max CFL* and $\overline{CFL}$ values are 8.07 and 3.35 respectively. As compared to GVF case, where the dispersion step can be neglected, one can find clearly that the restriction on the selection of time step becomes more rigid for the bend flow case, in which the dispersion step cannot be neglected. Nevertheless, it still allows for model users to select relatively high *Max CFL*, $\overline{CFL}$ and Δt values when IM model is adopted. The CPU time for a two hour simulation for each case is also shown in Table 2. With the same Δt, the IM model may require slightly more CPU time. Nevertheless, as Δt is greater than 2.59 s, EX model can no longer be converged for the simulation. On the other hand, IM model can be tolerant for even three times larger Δt with **a** very convincing convergent solution. From Table 2, with the use of maximum allowable Δt = 2.59 s for EX model and Δt = 9.45 s for IM model, one can find that the CPU time for IM model is only about one-third of that for EX model.

4.3 Shallow Recirculating Flow Case

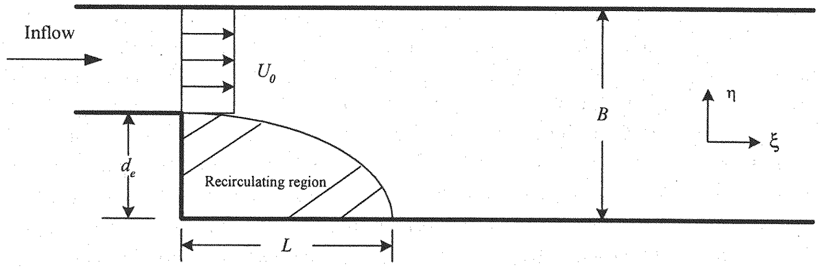

Fig. 5 Shallow recirculating flow produced by sudden widening of flow

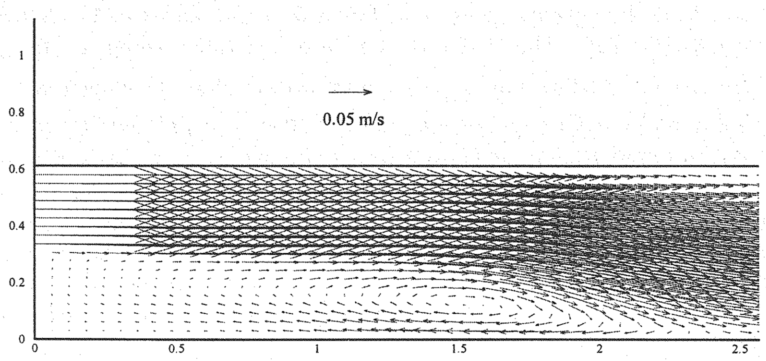

Fig. 6 Velocity vector field for the shallow recirculating flow case

Shallow recirculating flows are common occurrences in natural as can be observed in bays and harbors, behind islands, and around coastal inlets. Because of the simple geometry with recirculating zone for the experimental data conducted by Babarutsi *et al.* [15], it can be regarded as a typical test case for the model verification. The reicrculating flow in the experiment was produced by a sudden widening of the flow in the smooth channel. Fig. 4 shows a plan view of the geometry of the flow, in which L represents the recirculating length for recirculating zone. Flow entering the channel was blocked off on one side; forming a lateral expansion d_e as shown in Fig. 5. The width of the channel and the lateral expansion d_e were 0.61 m and 0.305 m respectively; the uniform velocity at inlet U_0 was 0.145 m/s; water depth d was 0.0819 m; friction factor C_f was 0.00527.

Table 3 Recirculating length and recirculating flow rate obtained by IM model, CV model, and experiment.

Experiment		Models			
		IM Model		CV Model	
L/d_e	q/U_0d_e	L/d_e	q/U_0d_e	L/d_e	q/U_0d_e
7.87	0.085	7.68	0.082	7.43	0.109

The feature of the shallow recirculating zone is characterized by the dimensionless recirculating length L/d_e and the dimensionless reverse-flow rate q/U_0d_e, in which q represents the maximum value of the reverse-flow rate per unit width. Table 3 shows the results of the experiment.

With a 81×20 uniformly distributed grid, the IM model (Δt = 0.4 s) is applied to predict the shallow recirculating flow field. The boundary conditions for upstream, downstream and banks are the inflow discharge per unit width, the measured water-surface elevation, and the no-slip condition respectively. The eddy viscosity υ

keeps constant throughout the recirculating flow field and can be determined as $\upsilon = 0.0067U_0 d_e$ [16]. The results of dimensionless recirculating length L/d_e and dimensionless reverse-flow rate $q/U_0 d_e$ from IM model are given in Table 3. From Table 3, IM model yields a fairly good prediction that is very close to the measurement, in which IM model slightly underestimates L/d_e and $q/U_0 d_e$ by 2.4 % and 3.5 % respectively. The result of velocity vector field simulated from IM model is shown in Fig. 6. One can observe from Fig. 6 that inflow is imposed at the upper half of the left side of the channel and a recirculating region forms at the lower half of the left side of the channel, near the sudden widening of the channel. Meanwhile, large velocity gradient is evident near the interface between upper and lower halves near the sudden widening of the channel.

Table 4 CPU time needed by IM and EX models for shallow recirculating flow case with various Δt

Δt(sec)	0.1		0.2		0.3		0.4		0.75	1.0	2.0	3.2
Model Type	EX	IM	EX	IM	EX	IM	EX	IM	IM	IM	IM	IM
CPU Time (sec)	3872	4300	1932	2246	1297	1502	977	1130	601	456	230	151
Max CFL	0.25		0.52		0.81		1.08		1.97	2.49	5.02	8.15
$\overline{CFL}$	0.14		0.26		0.39		0.53		1.00	1.31	2.61	4.17

The results of stability test for IM and EX models are shown in Table 4. However, the indexes of k_g and k_s are not suitable in the present case since the simulated results may have negative values or approach to zero. Therefore, only E_{rms} is adopted here for analysis. By regarding the results from IM model with $\Delta t = 0.4$ s as the observed results, which had been validated previously with good match with experimental data, it was found that the values of E_{rms} for each simulated case studied here are all less than a very small value (say about 5×10^{-3}). As one can observe from Table 4, the use of EX model has the more severe stability constraint in which the maximum values of *Max CFL*, $\overline{CFL}$ and Δt allowed are 1.08, 0.53 and 0.4 s respectively: In contrast, the IM model can be used with relatively large maximum values of *Max CFL*, $\overline{CFL}$ and Δt which are 8.15, 4.17 and 3.2 s respectively. It is obvious that the flow field of the shallow recirulating flow case is more complicated than that of the bend flow case since the flow directions are variant and the velocity gradient are greater in the former case. This complexity of flow field may cause more severe stability constraint for numerical simulation. Furthermore, if the maximum allowable $\Delta t = 0.4$ s is used for EX model and $\Delta t = 3.2$ s is used for IM model, from Table 4, one can find that the CPU time needed for a two hour simulation with IM model is about 6.4 times less than that with EX model.

4.4 Dam-Break Flow

Understanding the basic flow characteristics of dam-break problems is essential for more reliable engineering design. It is usual to regard the dam-break wave as an unsteady shallow water flow [17]. The flow is usually subcritical upstream of the dam site and is supercritical downstream. The numerical schemes used for solving the problem will face severe challenges especially when they are applied to cases with large initial water depth in the reservoir and zero depth, dry bed, in the downstream channel.

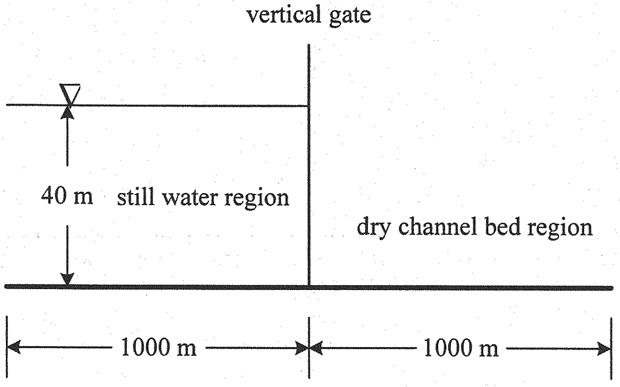

Fig. 7 Initial situation of the dam-break flow case

A hypothetic dam-break flow case with analytical solution proposed by Chow [18] is adopted herein to examine the robustness of IM model. The channel with vertical walls is 2000 m in length and 35 m in width. Bed slope and resistance are assumed to be negligible. The channel is rectangular in section and is initially closed by a transverse vertical gate, as shown in Fig. 7, containing still water, which the depth is 40m, on its left and having a dry channel bed on its right. The gate is located in middle of the channel, i.e., 1000 m from the upstream end, and is removed instantaneously. A uniform mesh of 201×36 is selected and the total simulation time is 20 s after the dam break.

The main difficulty in dealing with the propagation of a wave front on a dry bed lies in the boundary conditions of the flow field. The location of the propagating boundary is not known a priority nor is there any additional equations associated with flood wave propagation on an existing channel. In the present study, the distance between the upstream boundary and dam site is designed so as to ensure that the velocity is equal to zero at the upstream boundary site and the computational field during the total simulating time includes at least two more grid nodes in the ξ direction with zero depth of flow at the downstream boundary site [19]. Therefore, the discharge given at the upstream end and the water depth given at the downstream end of the channel are all set equal to zero. In such a situation, the velocity boundary conditions for dispersion step are no more unknown and they can be set as zero.

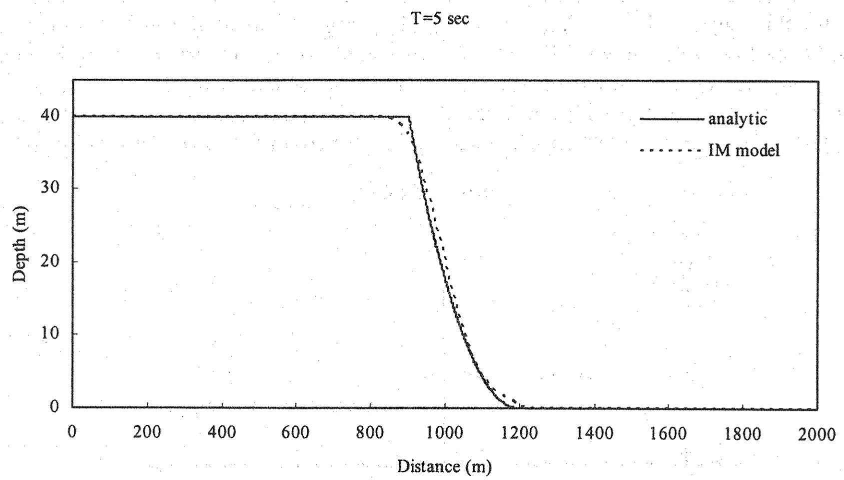
T=5 sec
analytic
IM model
Depth (m)
40
30
20
10
0
0
200
400
600
800
1000
1200
1400
1600
1800
2000
Distance (m)

(a)

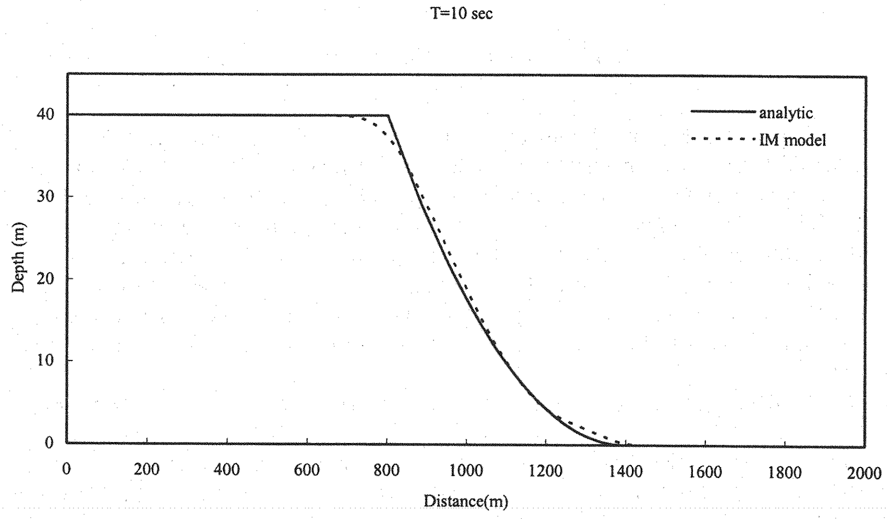
T=10 sec
analytic
IM model
Depth (m)
40
30
20
10
0
0
200
400
600
800
1000
1200
1400
1600
1800
2000
Distance(m)

(b)

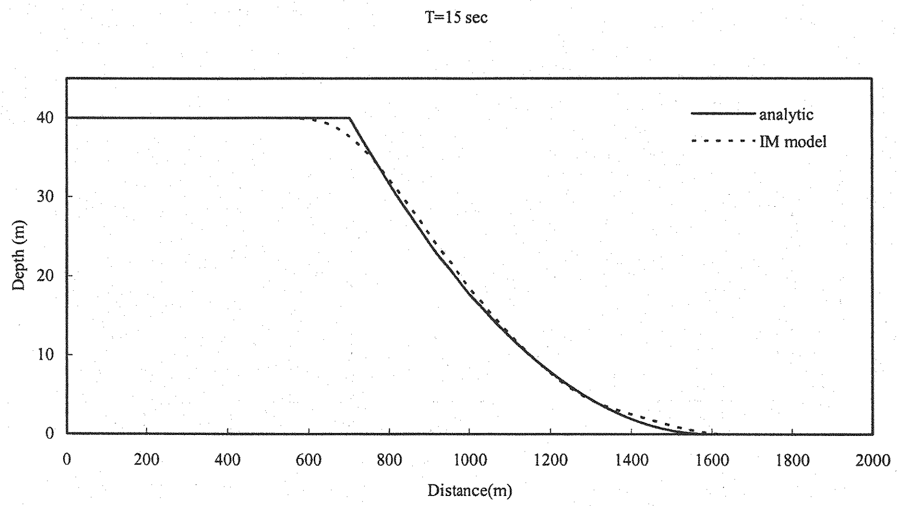

(c)

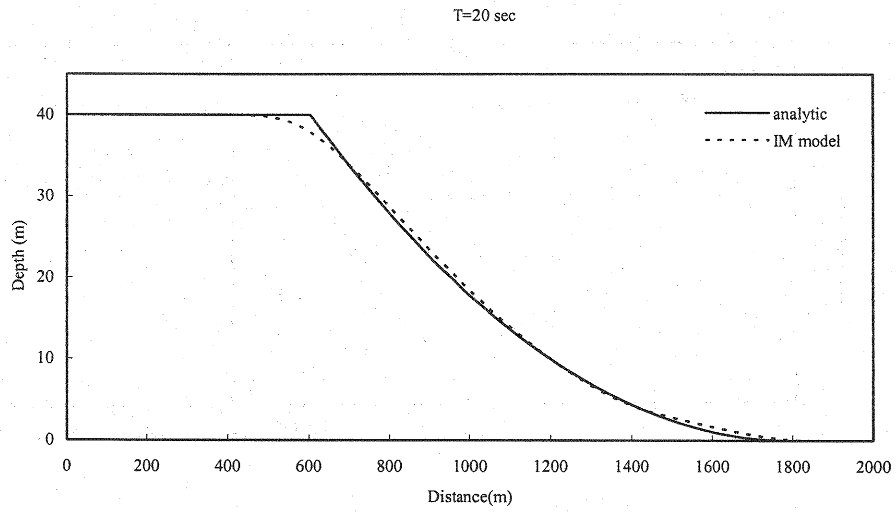

(d)

Fig. 8 Comparison between simulated depth and analytical solution at various time. (a) T = 5 s, (b) T = 10 s, (c) T=15 s, (d) T = 20 s.

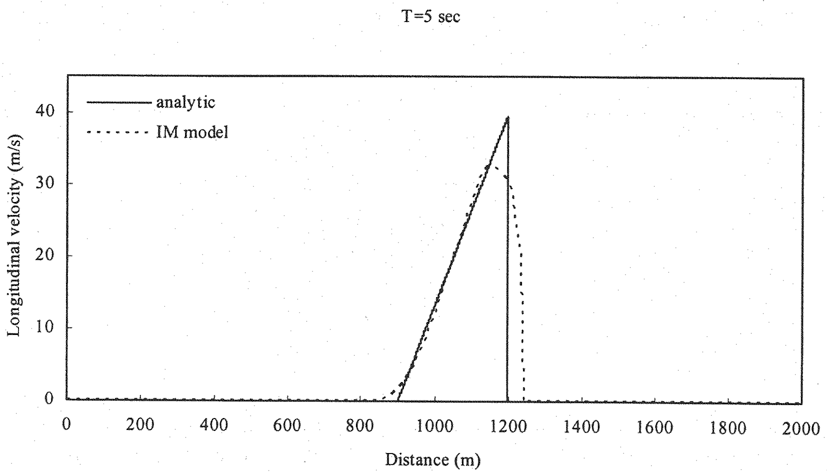
T=5 sec
analytic
IM model
Longitudinal velocity (m/s)
0
10
20
30
40
0
200
400
600
800
1000
1200
1400
1600
1800
2000
Distance (m)

(a)

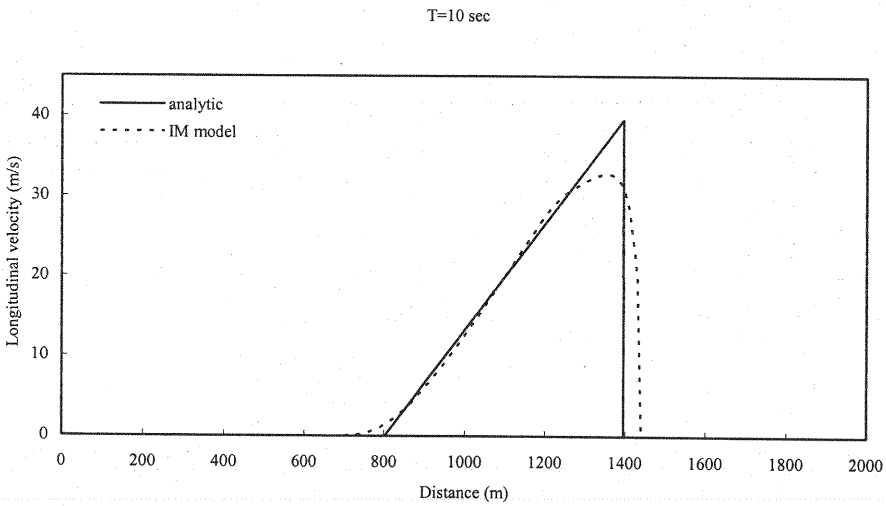
T=10 sec
analytic
IM model
Longitudinal velocity (m/s)
0
10
20
30
40
0
200
400
600
800
1000
1200
1400
1600
1800
2000
Distance (m)

(b)

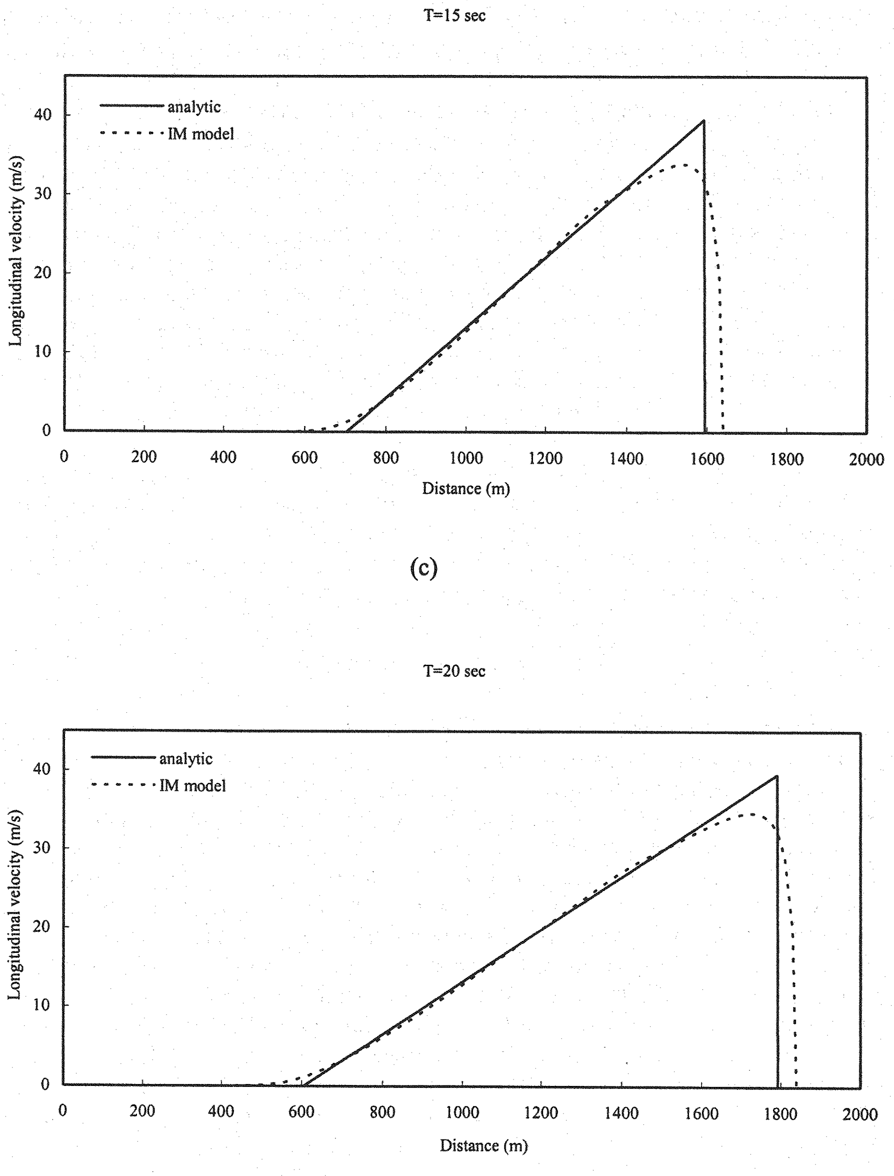

Fig. 9 Comparison between simulated longitudinal velocity and analytical solution at various time. (a) T = 5 s, (b) T = 10 s, (c) T=15 s, (d) T = 20 s.

Figs. 8(a)−(d) show the comparisons of water-surface profile along the channel centerline between the results from IM model (Δt = 0.25 s) and analytical solutions at 5, 10, 15, and 20 s respectively. Figs. 9(a)−(d) show the corresponding longitudinal velocity distributions along the channel centerline at 5, 10, 15, and 20 s respectively. One can observe from Figs. 8 and 9 that the simulated results agree fairly well with analytical solutions. From Figs. 8(a)−(d), a positive steep-front wave develops and propagates downstream, associated with a negative wave propagating oppositely upstream of the dam after the dam breaches. As time increases, the trailing edge recedes upstream and the wave front advances downstream. The water-surface profile is a parabola and smoothly tangential to the channel bed. Nevertheless, since the Hybrid scheme adopted by the present study has only a first-order accuracy, numerical damping is exhibited at the shock front as indicated both in Figs. 8 and 9. According to the above analyses, this application study demonstrates the ability of the IM model to deal with the mixed type of unsteady subcritical and supercritical flows and the channel bed being alternatively dry and wet.

By testing the numerical stability without having any oscillations or computational failure for IM model, the maximum time step that can be used in the present dam-break case is 0.25 s; yielding *Max CFL* of 0.89 and $\overline{CFL}$ of 0.31. In contrast, the EX model cannot work at all even if a very small time step 0.001 s is used. This shows the great advantage of the IM model because a relative large time step can be used in the numerical simulation with discontinuity and dry bed conditions.

5. CONCLUSIONS

An implicit two-step split-operator procedure for solving the shallow water flow equations has been presented in this paper. To show the need for an implicit scheme for practical use, an explicit type two-step model was developed herein for comparison. Four cases, including GVF, bend flow, shallow recirculating flow and dam-break flow, have been demonstrated to show the accuracy, flexibility and practical applicability of IM model. In the GVF case, in which the dispersion step can be neglected, the solutions can almost achieve unconditional stability by means of IM model. By using the maximum allowable time step for both models, the IM model is about 2.9 and 6.4 times faster than EX model for the bend flow and shallow recirculating flow case, respectively. The dam-break flow case demonstrates that IM model is capable of solving the mixed type of unsteady subcritical and supercritical flows and the channel bed being alternatively dry and wet with adequate accuracy. In short, our findings demonstrate that the implicit two-step split-operator approach proposed is a competitive scheme which is capable of being applied to various kinds of practical hydraulic problems.

ACKNOWLEDGMENTS

Partial financial support of this study from the National Science Council of Taiwan, R.O.C., through Contract NSC-88-2218-E009-032 is greatly appreciated. The computer resources used in this study were provided by the National Center for High-Performance Computing of Taiwan, R.O.C..

REFERENCES

1. McGuirk, J.J. and Rodi, W. : A depth-averaged mathematical model for the near field of side discharges into open channel flow, J. Fluid Mech., Vol.86, No.4, pp.761-781, 1978.
2. Molls, T. and Chaudhry, M.H. : Depth-averaged open-channel flow model, J. Hydr. Engrg., ASCE, Vol.121, No.6, pp.453-465, 1995.
3. Ye, J and McCorquodale, JA. : Depth-averaged hydrodynamic model in curvilinear collocated grid, J. Hydr. Engrg., ASCE, Vol.123, No.5, pp.380-388, 1997.
4. Lien, H.C. and Hsieh, T.Y. and Yang, J.C. : Use of two-step split-operator approach for 2D shallow water flow computation, Int. J. Numer, Methods in Fluids, Vol.30 pp.557- 575, 1999.
5. Rosenfeld, M. and Kwak, D. and Vinokur, M. : A fractional step solution method for the unsteady incompressible Navier-Stokes equations in generalized coordinate systems, J. Comput, Phys., Vol.94, pp.102-137, 1991.
6. Benque, J.P. and Cunge, J.A. Feuillet, J. and Hauguel, A. and Holly, F.M. : New method for tidal current computation, J. Waterw. Port Coast. Ocean Eng., ASCE, Vol.108, pp.396- 417,1982.
7. Kim, J. and Moin, P. : Application of a fractional-step method to incompressible Navier- Stokes equations, J. Comput. Phys., Vol.59, pp.308-323, 1985.
8. Preyret, R. and Taylor, TD. : Computational Methods for Fluid Flow, Springer, New York, pp.160-162, 1983.
9. Rastogi, A.K. and Rodi, W. : Prediction of Heat and Mass Transfer in Open Channels, J. Hydr. Div., ASCE, Vol.104, No.3, 397-420, 1978.
10. Falcon, A.M. : Analysis of flow in alluvial channel bends, PhD thesis, Dept. Mech. and Hydr. University of Iowa, Iowa City, Iowa, 1979.
11. de Vriend, H.J. : A mathematical model of steady flow in curved shallow channels, J. Hydr. Res., Delft, The Netherlands, Vol.15, No.1, pp.37-54, 1977.
12. Spalding, D.B. : A novel finite difference formulation for differential expressions involving both first and second derivatives, Int. J. Numer. Methods Eng., Vol.4, pp.551-559, 1972.
13. Leggett, R.W. and Williams, L.R. : A reliability index for models, Ecological Modelling, Vol.13, pp.303-312, 1981.
14. de Vriend, H.J. and Koch, F.G. : Flow of water in a curved open channel with a fixed plan bed, Rep. on Experimental and Theoretical Investigations R675-VM1415, Part I, Delft University of Technology, Delft, The Netherlands, 1977.
15. Babarusti, S. and Ganoulis, J. and Chu, V.H. : Experimental investigation of shallow recirculating flows, J. Hydr. Engrg., ASCE, Vol.115, No.7, pp.906-924, 1989.
16. Babarusti, S. and Nassiri, M. and Chu, V.H. : Computation of shallow recirculating flow dominated by friction, J. Hydr. Engrg., ASCE, Vol.122, No.7, pp.367-373, 1996.
17. Fraccarollo, L. and Toro, E.F. : Experimental and numerical assessment of the shallow water model for two-dimensional dam-break type problems, J. Hydr. Res., Vol.33, No.6, pp.843-863, 1996.
18. Chow, V.T. : Open-Channel Hydraulics, McGRaw-Hill, New York, Vol.568, 1959.
19. Bellos, C.V. : Sakkas JG. 1-D dam break flood-wave propagation on dry bed, J. Hydr. Engrg., ASCE, Vol.113, No.12, pp.1510-1524,1987.

(Received December 18, 2003 ; revised March 31, 2004)